THE ASTROPHYSICAL JOURNAL SUPPLEMENT SERIES, 30:247–258, 1976 March

ABSOLUTE CALIBRATION OF MILLIMETER-WAVELENGTH SPECTRAL LINES

B. L. ULICH
National Radio Astronomy Observatory,* Tucson, Arizona
AND
R. W. HAAS†
National Radio Astronomy Observatory, Charlottesville, Virginia
Received 1975 March 17

ABSTRACT

A detailed analysis of the chopper-wheel method of calibrating the intensity of a millimeter-wavelength spectral line is presented. Special techniques were used to construct a receiver which eliminates most of the usual calibration difficulties. The zenith atmospheric extinction between 3.5 mm and 2.6 mm wavelength was measured, and the intensities of six spectral lines in this range were absolutely calibrated with an estimated uncertainty (1 σ) of 7 percent. The effects of the antenna power pattern on the corrected antenna temperature T_A^* are calculated for several simple models of the source brightness distribution.

Subject headings: interstellar: molecules — radio sources: lines

I. INTRODUCTION

Many molecules known to exist in interstellar space have rotational transitions which lie in the millimeter-wavelength region of the electromagnetic spectrum. Since the discovery of CO in 1970 (Wilson *et al.* 1970), 23 molecular species have been detected at millimeter wavelengths using the NRAO 11 m radio telescope at Kitt Peak, Arizona. Observations of the intensities, frequencies, velocity structure, and polarizations of spectral lines of different molecules and of different transitions of the same molecule can be used to infer such physical conditions in interstellar clouds as temperature, density, velocity, and radiation fields. Already a wealth of data exists in the literature. (Zuckerman and Palmer [1974] have recently reviewed the published radio spectral line data.) However, these data can be fully understood only if they are calibrated in an absolute sense.

This paper reports the results of several experiments carried out between 1973 May and 1974 June with the NRAO 11 m antenna and millimeter-wavelength spectrometer. The goals were (1) to enable the maximum information to be extracted from existing data, (2) to provide absolute calibration sources for future work, and (3) to facilitate comparisons with data taken with other radio telescopes.

II. CALIBRATION THEORY

The most important parameters to be measured in a single observation of a spectral line are the intensity, line width, central frequency, and polarization. Most microwave transitions (except OH, H_2O [Litvak 1971], and possibly SiO masers) exhibit little or no polarization. In the following analysis, it is assumed that the spectral line radiation is randomly polarized. Most millimeter-wavelength spectrometers currently in use employ double sideband radio-frequency (RF) mixers with reflex klystrons as local oscillators. Thus both the upper and lower RF sidebands are down-converted to an intermediate frequency (IF) for subsequent amplification and detection. Frequency resolution is obtained through a bank of discrete band-pass filters centered at the IF. Spectra are produced by sequentially scanning the outputs of square-law detectors associated with each filter channel. Since the filter bank operates at a relatively low frequency, the response of each channel can be measured and adjusted to the desired band-pass shape and center frequency using conventional techniques. The radio frequency of the center of each sideband depends on both the local oscillator (LO) and first intermediate frequencies. The LO frequency is set by phase-locking the klystron to a harmonic of a stable lower frequency tunable oscillator. The accuracy of the sideband frequencies is typically a small fraction of the bandwidth of a single filter channel. Thus the spectrometer resolution usually determines both the accuracy and precision with which one can determine the frequency of a narrow spectral line.

When the IF is not a negligible fraction of the LO frequency, the signal and image sidebands (which are separated in frequency by twice the IF) are at appreciably different wavelengths. Waveguide components (including the mixer) in the RF section of the receiver will have frequency-dependent characteristics which may cause the

* The National Radio Astronomy Observatory is operated by Associated Universities, Inc., under contract with the National Science Foundation.

† Presently at the Max Planck Institute for Radio Astronomy, Bonn, Germany.

receiver to respond unequally to signals in the two sidebands. This complicates the receiver thermal calibration for spectral-line observations, since most calibration schemes involve either blackbody sources or broad-band plasma discharge tubes. That is, the calibration signal is simultaneously detected in both the signal and image sidebands, while the spectral line can be observed in the signal sideband only. Of course, if the relative receiver gains in the two sidebands were precisely known, then the calibration scale could be adjusted accordingly. However, a direct measurement at a few millimeters wavelength is not currently possible with sufficient precision. Therefore, other means must be found to avoid this calibration uncertainty before accurate intensity measurements can be made.

One method currently used to calibrate the intensity of millimeter-wavelength spectral lines is the rotating chopper-wheel (Penzias and Burrus 1973). A microwave absorber at ambient temperature is alternately introduced and removed at a point just in front of the antenna feed horn, resulting in a calibration signal equal to the temperature difference between the absorber and the antenna. This method produces a thermal scale corrected (to first order) for atmospheric extinction. As Davis and Vanden Bout (1973) have pointed out, however, the attenuation of the atmosphere is not completely accounted for, since (1) the mean atmospheric temperature is generally less than the ambient air temperature near ground level, and (2) the atmospheric extinction may differ in the two sidebands of the mixer receiver.

When the absorbing material on the chopper wheel at ambient temperature $T_{\rm amb}$ covers the feed horn aperture, the antenna temperature is

$$T_{\rm load} = G_s J(\nu_s, T_{\rm amb}) + G_i J(\nu_i, T_{\rm amb}) , \tag{1}$$

where G_s and G_i are the receiver power gains at the signal (ν_s) and image (ν_i) frequencies (normalized so that $G_s + G_i = 1$), and

$$J(\nu, T) = \frac{h\nu/k}{\exp(h\nu/kT) - 1} \tag{2}$$

is the effective radiation temperature of a blackbody source of temperature T. Here h is Planck's constant, ν is the applicable frequency, k is Boltzmann's constant, and T is the absolute temperature. With the absorber removed and the telescope pointed at blank sky, the antenna temperature at the prime focus is

$$T_{\rm sky} = G_s[\eta_l J(\nu_s, T_s) + (1 - \eta_l) J(\nu_s, T_{\rm sbr})] + G_i[\eta_l J(\nu_i, T_i) + (1 - \eta_l) J(\nu_i, T_{\rm sbr})] \tag{3}$$

where η_l is the telescope efficiency taking into account spillover, blockage, and ohmic losses. Thus

$$\eta_l = \eta_s \eta_{bl} \eta_r , \tag{4}$$

where η_s is the spillover efficiency, η_{bl} is the blockage efficiency, and η_r is the radiation efficiency, which includes ohmic losses in the antenna and absorption by paint on the reflector surface. $T_{\rm sbr}$ is the apparent brightness temperature of the received radiation which results from the spillover, blockage, and radiation losses. T_s and T_i are the sky brightness temperatures in the signal and image sidebands, and are given by

$$J(\nu_s, T_s) = J(\nu_s, T_{\rm m})[1 - \exp(-\tau_s A)] + J(\nu_s, T_{\rm bg}) \exp(-\tau_s A) , \tag{5}$$

and

$$J(\nu_i, T_i) = J(\nu_i, T_{\rm m})[1 - \exp(-\tau_i A)] + J(\nu_i, T_{\rm bg}) \exp(-\tau_i A) , \tag{6}$$

where $T_{\rm m}$ is the mean atmospheric temperature (assumed equal in the two sidebands), $T_{\rm bg}$ is the brightness temperature of the cosmic background radiation (Penzias 1972), τ_s and τ_i are the atmospheric zenith optical depths at the signal and image frequencies, and A is the air mass in the direction of observation.

The chopper-wheel calibration signal is the antenna temperature difference between the absorber and the antenna looking toward blank sky, and is given by

$$\begin{aligned} \Delta T_{\rm cal} \equiv T_{\rm load} - T_{\rm sky} = {} & G_s[J(\nu_s, T_{\rm amb}) - \eta_l J(\nu_s, T_s) - (1 - \eta_l) J(\nu_s, T_{\rm sbr})] \\ & + G_i[J(\nu_i, T_{\rm amb}) - \eta_l J(\nu_i, T_i) - (1 - \eta_l) J(\nu_i, T_{\rm sbr})] . \end{aligned} \tag{7}$$

When the antenna is pointed at a spectral line source, the antenna temperature at the prime focus is

$$\begin{aligned} T_{\rm source} = {} & G_s[\eta_l(1 - \eta_f) J(\nu_s, T_s) + \eta_l \eta_f \{J(\nu_s, T_E)[1 - \exp(-\tau)] \exp(-\tau_s A) \\ & + J(\nu_s, T_{\rm bg}) \exp(-\tau) \exp(-\tau_s A) + J(\nu_s, T_{\rm m})[1 - \exp(-\tau_s A)]\} \\ & + (1 - \eta_l) J(\nu_s, T_{\rm sbr})] + G_i[\eta_l J(\nu_i, T_i) + (1 - \eta_l) J(\nu_i, T_{\rm sbr})] , \end{aligned} \tag{8}$$

where T_E is the excitation temperature and τ the optical depth of the source. The forward beam coupling efficiency n_f is defined as

$$\eta_f \equiv \left[\iint_{\text{source}} P_n(\Psi - \Omega)B_n(\Psi)d\Psi\right] \Big/ \left[\iint_{2\pi} P_n(\Omega)d\Omega\right], \tag{9}$$

where P_n is the normalized antenna power pattern, B_n is the normalized apparent source brightness distribution, Ω is the direction of peak antenna gain, Ψ is the direction of maximum source brightness, and $d\Omega$ and $d\Psi$ are infinitesimal elements of solid angle. Note that the normalizing integral is only over the forward hemisphere (2π sr) rather than an entire sphere; this is a result of assuming that the radiation resulting from feed spillover and blockage originates entirely in the backward hemisphere and is applicable to prime focus observations. For a very extended, uniformly bright source, $B_n(\Psi) = 1$ and $\eta_f = 1$; i.e., the source completely fills the forward antenna beam with no dilution.

The antenna temperature difference between the source and blank sky is defined as

$$\Delta T_{\text{source}} \equiv T_{\text{source}} - T_{\text{sky}} = G_s\eta_l\eta_f \exp(-\tau_s A)(1 - e^{-\tau})[J(\nu_s, T_E) - J(\nu_s, T_{\text{bg}})]. \tag{10}$$

The corrected antenna temperature T_A^* of the source is defined as

$$T_A^* \equiv \Delta T_{\text{source}}/G_s\eta_l \exp(-\tau_s A) = (\Delta T_{\text{source}}/\Delta T_{\text{cal}})T_C, \tag{11}$$

where

$$T_C \equiv \Delta T_{\text{cal}}/[G_s\eta_l \exp(-\tau_s A)]. \tag{12}$$

Thus

$$T_A^* = \eta_f(1 - e^{-\tau})[J(\nu_s, T_E) - J(\nu_s, T_{\text{bg}})]. \tag{13}$$

Note that by proper choice of the equivalent calibration temperature T_C, T_A^* has been corrected for receiver gain (G_s), atmospheric extinction [$\exp(-\tau_s A)$], and antenna losses (η_l). In fact, T_A^* is simply the source antenna temperature one would measure outside the atmosphere with a lossless antenna and a single-sideband receiver. From an absolute calibration point of view, this is clearly the ideal case. From equation (11) it is evident that if T_C is known by previous measurement or calculation, one only needs to measure the ratio of the spectral line intensity to the calibration signal at the same air mass in order to find T_A^*, which will be independent of air mass. The corrected antenna temperature depends primarily on those factors which are influenced by the properties of the source (ν_s, τ, T_E, and B_n). Since T_A^* depends on η_f, which in turn depends on both the apparent source brightness distribution B_n and the antenna power pattern P_n, observations of the same source with different antennas (with different power patterns) will in general yield different values of T_A^*. A fairly detailed knowledge of the power patterns of each antenna and of the source brightness distribution is needed to make meaningful comparisons. Only if the source were spatially very extended and uniformly bright (so that $\eta_f = 1$) would T_A^* be independent of the antenna properties. If, in addition, $h\nu_s/kT_A^* \ll 1$, then $T_A^* \approx T_B$, where the excess line brightness temperature T_B is defined as

$$J(\nu_s, T_B) \equiv (1 - e^{-\tau})[J(\nu_s, T_E) - J(\nu_s, T_{\text{bg}})]. \tag{14}$$

Combining equations (13) and (14) produces the general relation between corrected antenna temperature and the excess brightness temperature of the spectral line (assuming no continuum radiation from the source),

$$T_A^* = \eta_f J(\nu_s, T_B). \tag{15}$$

Substituting equation (7) into equation (12) results in a general expression for T_C:

$$\begin{aligned} T_C = {} & J(\nu_s, T_{\text{sbr}}) - J(\nu_s, T_{\text{bg}}) + (G_i/G_s)[J(\nu_i, T_{\text{sbr}}) - J(\nu_i, T_{\text{bg}})] \\ & + [\exp(\tau_s A) - 1]\{J(\nu_s, T_{\text{sbr}}) - J(\nu_s, T_{\text{m}}) + (G_i/G_s)[J(\nu_i, T_{\text{sbr}}) - J(\nu_i, T_{\text{m}})]\} + (G_i/G_s) \\ & \times \{\exp[(\tau_s - \tau_i)A] - 1\}[J(\nu_i, T_{\text{m}}) - J(\nu_i, T_{\text{bg}})] + [\exp(\tau_s A)/\eta_l] \\ & \times \{J(\nu_s, T_{\text{amb}}) - J(\nu_s, T_{\text{sbr}}) + (G_i/G_s)[J(\nu_i, T_{\text{amb}}) - J(\nu_i, T_{\text{sbr}})]\}. \end{aligned} \tag{16}$$

If the IF is small compared with the LO frequency, then $J(\nu_i, T) \approx J(\nu_s, T)$ and equation (16) reduces to

$$\begin{aligned} T_C \approx {} & (1 + G_i/G_s)[J(\nu_s, T_{\text{m}}) - J(\nu_s, T_{\text{bg}})] \\ & + (1 + G_i/G_s)[\exp(\tau_s A)][J(\nu_s, T_{\text{sbr}}) - J(\nu_s, T_{\text{m}})] \\ & + (G_i/G_s)\{\exp[(\tau_s - \tau_i)A] - 1\}[J(\nu_s, T_{\text{m}}) - J(\nu_s, T_{\text{bg}})] \\ & + (1 + G_i/G_s)[\exp(\tau_s A)/\eta_l][J(\nu_s, T_{\text{amb}}) - J(\nu_s, T_{\text{sbr}})]. \end{aligned} \tag{17}$$

The first term in equation (17) is the constant scale factor independent of atmospheric attenuation for which the chopper-wheel method was designed. The second term corrects for the fact that the mean atmospheric temperature is different from the spillover temperature, and the third term is the correction for different optical depths in the two sidebands. The fourth term in equation (17) corrects for the temperature difference between the rotating absorber and the spillover radiation. The result of Davis and Vanden Bout (1973) is identical to equation (17) under the additional assumptions that (1) the cosmic background radiation is negligible, (2) $h\nu_s \ll kT$ so that the Rayleigh-Jeans approximation to the Planck law is valid [i.e., $J(\nu_s, T) \approx T$], and (3) the equivalent spillover brightness temperature $T_{\rm sbr}$ is equal to $T_{\rm amb}$. At a few millimeters wavelength these assumptions (especially the last one) may not be valid, with the result that some systematic calibration error may be introduced.

The chopper-wheel calibration temperature depends on nine variables in equation (16): $T_{\rm amb}$, $T_{\rm m}$, $T_{\rm sbr}$, $T_{\rm bg}$, G_i/G_s, τ_s, τ_i, A, and η_l (it is assumed that the frequencies are already known). Several of these quantities can be easily measured or calculated, but others are difficult to determine directly, particularly those which vary with frequency. Thus evaluating equation (16) directly to obtain T_C is a formidable task. A simpler method which reduces the number of unknowns to be determined is to evaluate T_C using the definition of equation (12). That is, one must now measure only $\Delta T_{\rm cal}$ (at each of the air masses at which sources are to be observed), τ_s, η_l, and G_s. This need be done only once, since *under clear sky conditions* at high altitude sites the variability of the atmospheric attenuation at millimeter wavelengths will generally produce only minor errors in the corrected antenna temperature scale. Thus one can determine T_C once as a function of air mass at given IF and LO frequencies and use these values for all future observations with the same equipment without appreciable calibration error.

Once the corrected antenna temperature scale is established, the next step is to convert T_A^* to the physically meaningful brightness temperature. From other work we know that $T_{\rm bg} = 2.8$ K (Penzias 1972). In equation (13) there are now only three unknowns: η_f, τ, and T_E. The forward beam coupling efficiency can be calculated using equation (9) if the antenna power pattern P_n and source brightness distribution B_n are known. If the source is larger than the main lobe of the power pattern, B_n can be approximated by a normalized spatial map of T_A^* over the source. If the source is smaller than the main lobe, then $P_n \approx 1$ over the source and

$$\eta_f \approx A_e\Omega_s/\eta_l\lambda_s^2 , \tag{18}$$

where A_e is the effective collecting area of the telescope, λ_s is the wavelength corresponding to ν_s, and the source solid angle Ω_s is defined as

$$\Omega_s \equiv \int\int_{\rm source} B_n(\Psi)d\Psi . \tag{19}$$

In this case the source flux density S is given by

$$S = 2k\eta_l T_A^*/A_e . \tag{20}$$

Combining equations (13), (18), and (20) results in the usual expression for flux density:

$$S = \frac{2k\Omega_s}{\lambda_s^2}(1 - e^{-\tau})[J(\nu_s, T_E) - J(\nu_s, T_{\rm bg})] . \tag{21}$$

The problem of separating T_E and τ still remains, however, and they cannot be uniquely determined from a single observation of T_A^*. Only if other data (such as the relative intensities of different spectral lines) provide an independent measurement of either τ or T_E can both parameters be determined.

III. INSTRUMENTATION

The antenna used for these experiments is the NRAO 11 m diameter paraboloid located at an altitude of 1920 m on Kitt Peak in Arizona. The effective reflector tolerance (Ruze 1966) derived from radiometric gain measurements is 0.15 mm, and the absolute pointing accuracy is 7″ rms. Between 3.5 mm and 2.6 mm wavelength, the aperture efficiency decreases from 0.39 to 0.32 ($\pm$0.03), and the HPBW decreases from 78″ to 64″ ($\pm$2″). For these observations the radiometer was located at the focus of the 0.8 f/D primary reflector. The antenna feeds were conical horns dimensionally scaled with wavelength to produce identical radiation patterns at each spectral line frequency. The feed illumination patterns were measured and the results used to calculate the spillover efficiency (0.83 $\pm$ 0.04) and the blockage efficiency (0.88 $\pm$ 0.02). Taking into account the measured RF absorption by paint on the reflector surface, the radiation efficiency was estimated to be 0.99 $\pm$ 0.01. Thus from equation (4) the overall telescope efficiency η_l is 0.72 $\pm$ 0.04 and is independent of wavelength.

The radiometer was a double sideband mixer receiver with an IF of 1390 MHz and a fundamental klystron LO phase-locked to harmonics of a stable oscillator near 2 GHz. Interchangeable band-pass filters located between the feed horn and the RF mixer were used to provide image rejection. These coupled cavity waveguide filters have insertion losses between 0.9 dB and 2.8 dB in the signal sideband and rejections greater than 20 dB in the image sideband. Thus the overall radiometer was effectively a single-sideband receiver, which considerably

TABLE 1

CALIBRATED MOLECULAR LINES

Molecule	Transition Quantum Numbers	Frequency (GHz)	Wavelength (mm)
SiO.....	$v = 1, J = 2$–1	86.24328	3.48
HCN.....	$v = 0, J = 1$–0, $F = 1$–1	88.63042	3.38
	$v = 0, J = 1$–0, $F = 2$–1	88.63185	3.38
	$v = 0, J = 1$–0, $F = 0$–1	88.63394	3.38
X-ogen.....	Unknown	89.1885	3.36
$^{12}C^{18}O$.....	$v = 0, J = 1$–0	109.78218	2.73
$^{13}C^{16}O$.....	$v = 0, J = 1$–0	110.20137	2.72
$^{12}C^{16}O$.....	$v = 0, J = 1$–0	115.27120	2.60

simplified the problems of absolute intensity calibration. The receiver responded to linearly polarized radiation with the electric vector oriented parallel to the horizon. The single-sideband system noise temperature (including feed and filter losses) varied from 2000 K to 3500 K, depending on the frequency. The absolute antenna temperature scale was determined by alternately placing microwave absorbers at ambient temperature and at 77 K (the boiling point of liquid nitrogen) over the feed horn. The absorbing material used (Emerson and Cuming type CV-3) has a power reflectivity less than -40 dB at frequencies near 100 GHz and is assumed to radiate like a perfect blackbody. Relative intensity calibration was accomplished by synchronously detecting a chopper wheel in the aperture plane of the feed horn. The system performance was monitored during each chopper-wheel calibration by calculating the effective system temperature T_S according to the equation

$$T_S \equiv \frac{(T_R + T_{\rm sky})T_C}{(T_R + T_{\rm load}) - (T_R + T_{\rm sky})} \equiv \frac{T_R + T_{\rm sky}}{G_s \eta_l \exp(-\tau_s A)}, \tag{22}$$

where T_R is the single sideband noise temperature of the receiver. T_S is simply the single-sideband system temperature on the same corrected antenna temperature scale as the spectral line intensity (i.e., corrected for antenna and atmospheric losses).

The spectrometer consisted of a 256 channel filter bank with a filter width and spacing of 100 kHz. The corresponding velocity resolution at 3 mm wavelength is 0.3 km s^{-1}. The nonlinearity of the square-law detectors was measured to be less than 2 percent over the normal range of operation. During source observations the klystron was usually frequency-switched 30 MHz so that the reference spectrum did not overlap the 25.6 MHz instantaneous RF bandwidth of the filter bank. Spectra were produced by synchronously detecting each of the 256 detector outputs of the filter bank in phase with the frequency switching. For narrow lines the klystron was switched ± 6.4 MHz about the nominal LO frequency, thus shifting the line within the filter bank. The resulting spectrum was later shifted in frequency by 12.8 MHz and subtracted from itself in order to reduce the random receiver noise.

IV. OBSERVATIONS

The principal purpose of this experiment was to calibrate the absolute intensities of known millimeter-wavelength spectral lines. Six transitions of relatively abundant molecules in the 2.6 mm to 3.5 mm wavelength range were chosen: $^{12}C^{16}O$, $^{13}C^{16}O$, $^{12}C^{18}O$, X-ogen, HCN, and SiO. The transition frequencies and quantum numbers are given in Table 1. Seven standard molecular line sources were observed. Their epoch 1950.0 equatorial coordinates are listed in Table 2. These selected sources are approximately evenly spaced in right ascension and cover a wide range in declination. We were unable to observe all six molecules in every source because of the long integration times required for precise measurements. However, we obtained relatively good sky coverage for the HCN, X-ogen, and $^{12}C^{16}O$ lines.

TABLE 2

STANDARD MOLECULAR LINE SOURCES

Source	α(1950)	δ(1950)
W3(OH).....	$2^h23^m16^s.7$	$+61°38'54''$
Orion A.....	5 32 47.0	-5 24 21
IRC+10216....	9 45 14.8	$+13$ 30 40
W Hydra.....	13 46 12.0	-28 7 6
M17SW.....	18 17 26.5	-16 14 54
W51.....	19 21 27.0	$+14$ 24 30
S146.....	22 47 30.0	$+59$ 39 0

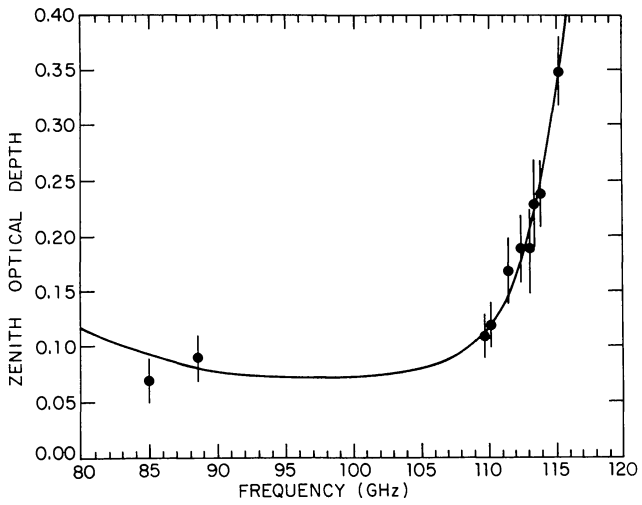

FIG. 1.—Measurements of atmospheric absorption in the 3 mm wavelength window. The solid curve is a theoretical prediction for 2 km altitude and 2 mm precipitable H_2O (Waters 1975).

a) Atmospheric Extinction

The zenith optical depth of the Earth's atmosphere varies considerably across the 3 mm wavelength window. A precise knowledge of the extinction at each frequency in Table 1 is necessary to determine the equivalent calibration temperature T_C (see eq. [12]) for each spectral line. We made extinction measurements from Kitt Peak at 10 frequencies between 85 GHz and 116 GHz under typical clear sky conditions. The ambient temperature was between 285 K and 295 K and the relative humidity was in the range 20–30 percent. Strong continuum sources (such as the Moon or Jupiter) were observed at different elevation angles with the single-sideband receiver, and the variation of antenna temperature with air mass was used to calculate the extinction. The data are plotted in Figure 1 along with the curve theoretically predicted for this altitude ($\sim$2 km) and 2 mm precipitable H_2O (Waters 1975). The agreement is surprisingly good considering the fact that the measurements were made on many different days and that no attempt has been made to correct the observations for variations in the precipitable water-vapor content of the atmosphere. The rapid variation of atmospheric extinction with frequency in the steep wing of the 118.75 GHz O_2 line (Tolbert *et al.* 1964) considerably complicates the calibration of the double-sideband receivers generally used for CO observations (Davis and Vanden Bout 1973). By using a single sideband receiver, we have avoided not only the problem of determining the receiver gain in the image sideband, but also the necessity of measuring the atmospheric extinction at the image frequency.

b) Spectral Lines

We determined the equivalent chopper-wheel temperature T_C at each frequency listed in Table 1 by directly evaluating equation (12). Since the RF band-pass filters reject the image sideband, $G_i = 0$ and thus $G_s = 1$. As discussed in § III, the telescope efficiency η_l is independent of wavelength for the frequency-scaled feed horns we used and has a calculated value of 0.72 ± 0.04. The atmospheric zenith optical depth τ_s was determined by the measurements plotted in Figure 1. At each spectral line frequency we also measured $\Delta T_{\rm cal}$ at several elevation angles between 18° and 90° and calculated the corresponding values of the air mass A. We found that the chopper-wheel calibration temperature (for observations at the prime focus of the NRAO 11 m telescope) could be closely approximated by

$$T_C = 250 + 36 \exp(\tau_s A), \tag{23}$$

and this expression was actually used to calibrate the corrected antenna temperature of each molecular line according to equation (11). Table 3 lists the measured parameters of each source observation. The radial velocity is the velocity at the peak line intensity away from the local standard of rest. The line width is the velocity width at one-half the peak intensity. T_A^* is the peak excess antenna temperature of the line corrected for antenna and atmospheric losses. The random error in T_A^* is the standard error due to receiver noise. Errors in the calculation of η_l and in the measurements of τ_s and $\Delta T_{\rm cal}$ produce an additional absolute calibration uncertainty of about 7 percent. The total error listed in Table 3 is the quadratic sum of the receiver noise and the absolute calibration error.

The $J = 1$–0 line of carbon monoxide (Wilson *et al.* 1970) has proved to be a most useful tool for probing galactic structure. Thus we observed the three most abundant isotopes in a variety of sources. Figures 2, 3, and 4 are the spectra obtained for $^{12}C^{16}O$, $^{13}C^{16}O$, and $^{12}C^{18}O$, respectively, in the direction of Becklin's star in the Orion Nebula.

TABLE 3

OBSERVED LINE PARAMETERS

Source	Radial Velocity* (km s^{-1})	Line Width† (km s^{-1})	T_A* (K)	Random Error‡ (K)	Total Error§ (K)
		SiO			
Orion A	-8.0	1.8	10.2	0.4	0.8
(18 May 1974)	-6.9	1.8	10.2	0.4	0.8
	+13.3	1.8	12.3	0.4	0.9
	+14.7	1.8	11.6	0.4	0.9
	+16.4	1.8	17.4	0.4	1.3
W Hydra	+38.3	2.3	15.8	0.3	1.1
(19 May 1974)	+40.8	2.3	6.9	0.3	0.6
	+44.6	2.3	3.0	0.3	0.4
		HCN			
Orion A	+9.4 (F=0-1)	4.7	6.8	0.5	0.7
	+9.4 (F=2-1)	4.7	17.2	0.5	1.3
	+9.4 (F=1-1)	4.7	9.6	0.5	0.8
IRC+10216	-21.8 (Unresolved)	≈ 24	3.5	0.3	0.4
M17SW	+19.2 (Unresolved)	≈ 16	6.9	0.4	0.6
W51	+53.7 (Unresolved)	≈ 19	3.7	0.3	0.4
		X-OGEN			
W3(OH)	-48.0	5.0	2.8	0.2	0.3
Orion A	+9.5	3.9	10.8	0.4	0.9
M17SW	+19.3	7.2	3.8	0.2	0.3
W51	+57.1	9.7	4.5	0.3	0.4
		$^{12}C^{18}O$			
Orion A	+9.0	6.0	2.1	0.2	0.2
M17SW	+19.4	6.2	2.2	0.3	0.3
		$^{13}C^{16}O$			
W3(OH)	-47.4	6.4	7.1	0.3	0.6
Orion A	+9.0	4.1	9.3	0.5	0.8
M17SW	+19.4	5.6	13.7	0.5	1.1
		$^{12}C^{16}O$			
W3(OH)	-47.4	6.8	16.1	0.7	1.3
Orion A	+9.0	6.3	60.0	2.0	4.7
IRC+10216	-26.0	26.7	4.2	0.4	0.5
M17SW	+19.4	8.5	39.5	2.0	3.4
W51	+57.1	12.5	28.4	0.8	2.1
	+68.9	5.6	10.7	0.8	1.1
S146	-49.6	4.5	13.2	1.0	1.4

*One standard deviation ≈ 0.8 km s^{-1}.
†One standard deviation ≈ 0.4 km s^{-1}.
‡The random error is the standard deviation of T_A* due to receiver noise.
§The total error of T_A* is the quadrature sum of the random error and the estimated 7% absolute calibration error.

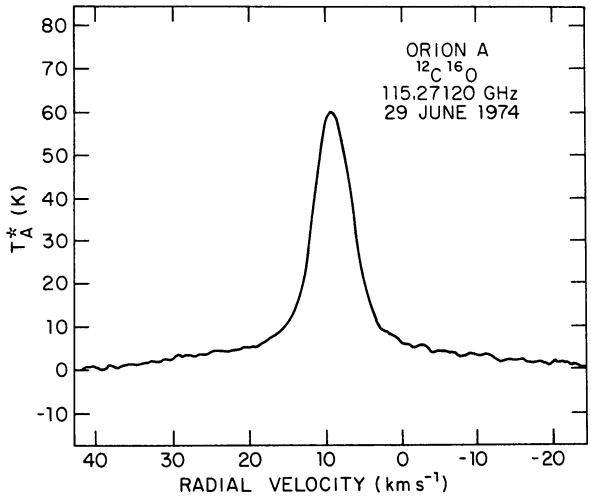

FIG. 2.—Spectrum of the $J = 1$–0 transition of $^{12}C^{16}O$ in Orion A. The abscissa is radial velocity with respect to the local standard of rest (LSR) calculated for a rest frequency of 115.27120 GHz. The ordinate is antenna temperature corrected for antenna and atmospheric losses.

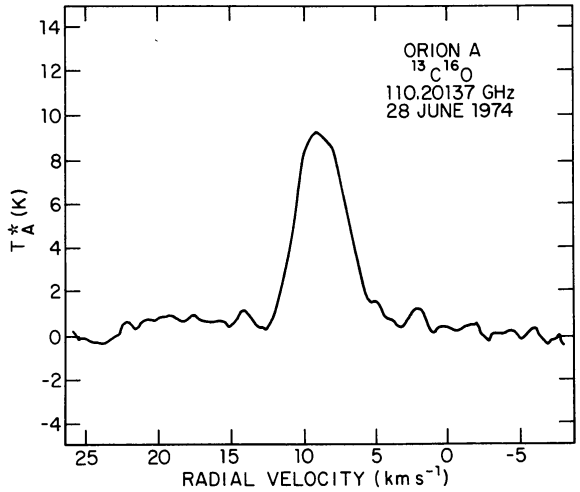

FIG. 3.—Spectrum of the $J = 1$–0 transition of $^{13}C^{16}O$ in Orion A. The abscissa is radial velocity with respect to the LSR calculated for a rest frequency of 110.20137 GHz. The ordinate is corrected antenna temperature.

X-ogen was the first unidentified microwave interstellar line (Buhl and Snyder 1970) and is now known to be a fairly common constituent of the interstellar medium (Buhl and Snyder 1973). The $v = 0$, $J = 1$–0 transition of HCO^+ was suggested as a candidate in 1970 (Klemperer 1970), and new evidence to support this identification was recently discovered (Snyder *et al.* 1975*a*). Figure 5 shows the Orion A spectrum of X-ogen assuming a rest frequency of 89.1885 GHz.

The $J = 1$–0 transition of HCN (Snyder and Buhl 1971) in the direction of Orion A is shown in Figure 6. The relatively narrow filters (100 kHz bandwidth and separation) used in the spectrometer allowed us to resolve the quadrupole hyperfine components in the Orion Nebula. In the other sources we observed, however, the hyperfine components are blended together, and we can determine only the intensity at the frequency of the strongest ($F = 2$–1) component.

The $v = 1, J = 2$–1 transition of SiO at 86.24328 GHz was discovered to be masing in Orion A in 1973 December (Snyder and Buhl 1974). Our calibration observations in 1974 May are shown in Figure 7. There is some indication that the relative intensities of several of the different velocity components had changed since 1973 December. Further observations in 1974 September confirmed the reality and time scale (months) of these small changes. Spectra taken in 1974 October, however, indicated the appearance of a broad underlying emission pedestal. This new feature, which is shown in Figure 8 with twice the velocity coverage as the previous spectrum, has an intensity of about 6 K and a width of about 35 km s^{-1}. It extends from about -20 to $+30$ km s^{-1} and includes all known velocity components of the SiO, H_2O, and OH masers (Snyder and Buhl 1975). A similar emission plateau has been observed in several SO_2 lines in the Orion Nebula (Snyder *et al.* 1975*b*). If the individual narrow lines are due to localized maser action at points within a gaseous envelope surrounding a variable late-type star, then the broad emission feature could be due to masing action throughout the entire expanding shell.

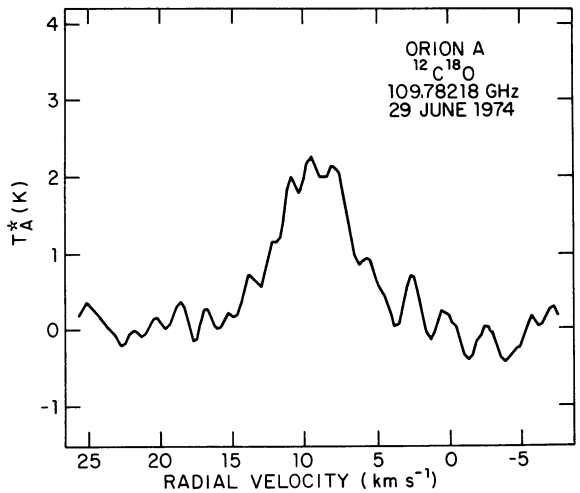

FIG. 4.—Spectrum of the $J = 1$–0 transition of $^{12}C^{18}O$ in Orion A. The abscissa is radial velocity with respect to the LSR calculated for a rest frequency of 109.78218 GHz. The ordinate is corrected antenna temperature.

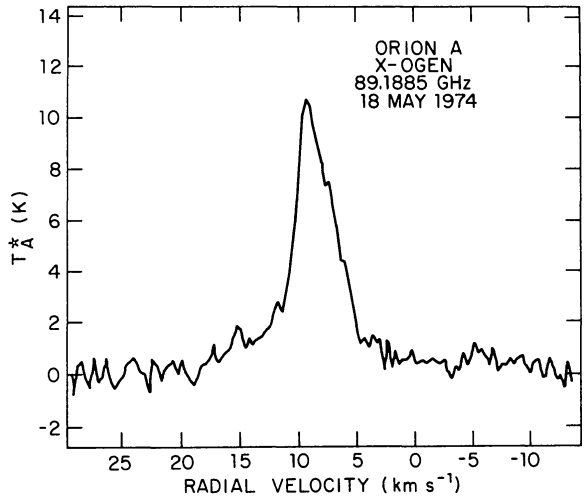

FIG. 5.—Spectrum of X-ogen in Orion A. The abscissa is radial velocity with respect to the LSR calculated for a rest frequency of 89.1885 GHz. The ordinate is corrected antenna temperature. X-ogen is probably the $v = 0, J = 1$–0 transition of HCO^+ (Snyder *et al.* 1975*a*).

V. DISCUSSION

The corrected antenna temperature T_A^* of a spectral line has been corrected for antenna and atmospheric losses. However, it still depends on the antenna power pattern through the forward beam coupling efficiency η_f. We must determine η_f in order to find the equivalent brightness temperature of the source. First we model the antenna power pattern using simple analytic functions. Next we consider several models of possible source brightness distributions. Finally, we derive expressions for η_f using the definition of equation (9) and illustrate their use with several examples.

At 3 mm wavelength the NRAO 11 m reflector antenna is not diffraction-limited. Surface errors correlated over regions appreciable in size compared with the antenna diameter scatter power near the electrical axis and produce an error pattern which must be accounted for in analyzing observations of extended sources (Ade *et al.* 1974). The simplest reasonable model of the actual antenna power pattern is the sum of two Gaussian functions (Harten 1973). The normalized power pattern P_n in x, y orthogonal coordinates is now given by

$$P_n(x, y) = A_D \exp\left[-4 \ln 2 \left(\frac{x^2 + y^2}{\theta_D^2}\right)\right] + A_E \exp\left[-4 \ln 2 \left(\frac{x^2 + y^2}{\theta_E^2}\right)\right], \quad (24)$$

where A_D and A_E are the amplitudes (normalized so that $A_D + A_E = 1$) and θ_D and θ_E are the half-power widths of the diffraction and error beams, respectively. The diffraction beam is narrow and large in amplitude; the error beam is much weaker but very broad compared with the main lobe. Using the procedure outlined by Baars (1973),

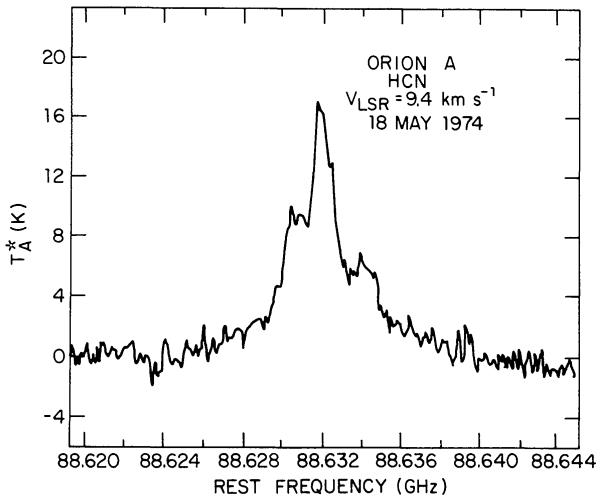

FIG. 6.—Spectrum of the $J = 1$–0 transition of HCN in Orion A. The abscissa is the rest frequency assuming a radial velocity of 9.4 km s^{-1} with respect to the LSR. The $F = 1$–1, $F = 2$–1, and $F = 0$–1 hyperfine components are at 88.63042, 88.63185, and 88.63394 GHz, respectively. The ordinate is corrected antenna temperature.

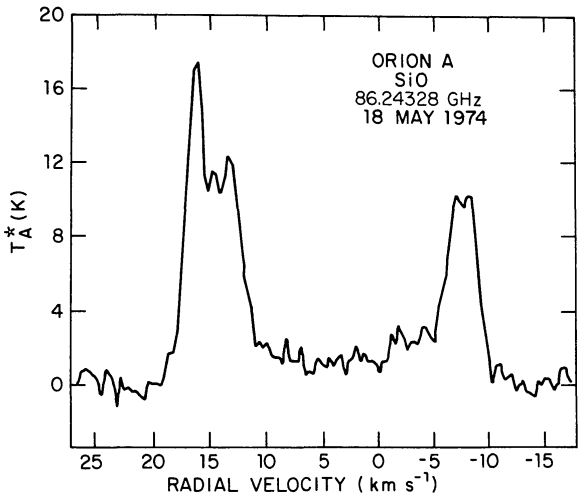

FIG. 7.—Spectrum of the $v = 1, J = 1$–0 transition of SiO in Orion A on 1974 May 18. The abscissa is radial velocity with respect to the LSR calculated for a rest frequency of 86.24328 GHz. The ordinate is corrected antenna temperature.

we estimate that at 2.6 mm wavelength (corresponding to the $^{12}C^{16}O$ line) $\theta_D = 1'.1$, $\theta_E = 25'$, $A_D = 0.9992$, and $A_E = 8 \times 10^{-4}$ for the NRAO 11 m telescope. Thus even though the error beam is at -31 dB with respect to the main beam, it receives significant power because of its large width. When a very extended source is observed at this wavelength, about 70 percent of the available power is received in the diffraction lobe and 30 percent in the error pattern.

For a uniformly bright circular disk source of radius R, the normalized source brightness distribution is

$$B_n(x, y) = 1 \text{ for } (x^2 + y^2)^{1/2} \leq R,$$
$$0 \text{ for } (x^2 + y^2)^{1/2} > R. \tag{25}$$

Substituting equations (24) and (25) into equation (9) results in the following general expression for n_f when the antenna beam is centered on the disk:

$$\eta_f = \frac{A_D\theta_D^2\{1 - \exp[-4 \ln 2(R/\theta_D)^2]\} + A_E\theta_E^2\{1 - \exp[-4 \ln 2(R/\theta_E)^2]\}}{A_D\theta_D^2 + A_E\theta_E^2}. \tag{26}$$

For the Sun or Moon $R = 15'$ and at 2.6 mm wavelength $\eta_f = 0.89$. Thus, even though the main beam is only $1'.1$ wide, about 11 percent of the available signal is lost in the far wings of the error pattern and is not received by the feed horn. As a calibration check we observed the center of the Moon at a phase angle of 43° past full and

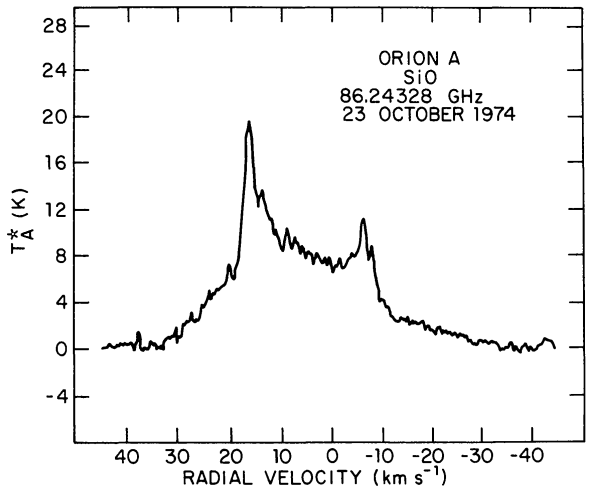

FIG. 8.—Spectrum of the $v = 1, J = 1$–0 transition of SiO in Orion A on 1974 October 23. The abscissa is radial velocity with respect to the LSR calculated for a rest frequency of 86.24328 GHz. The ordinate is corrected antenna temperature. Note the broad emission pedestal which is not present in Fig. 7.

measured $T_A^* = 269 \pm 19$ K at 2.6 mm wavelength. From equation (13) we calculate a disk brightness temperature of 306 ± 21 K. At 3.1 mm wavelength the corresponding temperature is 297 ± 12 K (Ulich *et al.* 1974), and at shorter wavelengths the temperature at this phase angle should be slightly higher. The good agreement of the two measurements indicates that for extended sources the absolute calibration scale is accurate within the estimated error. Observations of Jupiter when its mean semidiameter was 20″.1 resulted in a $T_A^* = 26 \pm 2$ K. From equation (26) we calculate $\eta_f = 0.16$, and from equation (13) we get a disk brightness temperature of 166 ± 13 K. The average of previous 2.1 mm and 3.1 mm absolute continuum measurements (Ulich *et al.* 1973; Ulich 1974) is 174 ± 12 K, which agrees within the errors with the chopper-wheel calibrated temperature. Thus the accuracy of the absolute calibration of our spectral line data is confirmed by observations of both extended and "point" continuum sources.

A Gaussian source of widths θ_x and θ_y has the brightness distribution function

$$B_n(x, y) = \exp\left\{-4 \ln 2\left[\left(\frac{x}{\theta_x}\right)^2 + \left(\frac{y}{\theta_y}\right)^2\right]\right\}. \quad (27)$$

Substituting equations (24) and (27) into equation (9) results in the following general expression for η_f when the antenna beam is centered on the peak of a Gaussian source:

$$n_f = \left[\left[\frac{A_D\theta_D^2}{\{[1 + (\theta_D/\theta_x)^2][1 + (\theta_D/\theta_y)^2]\}^{1/2}} + \frac{A_E\theta_E^2}{\{[1 + (\theta_E/\theta_x)^2][1 + (\theta_E/\theta_y)^2]\}^{1/2}}\right]\right] \Big/ (A_D\theta_D^2 + A_E\theta_E^2). \quad (28)$$

We mapped the $^{12}C^{16}O$ line at more than 20 points near the carbon star IRC+10216. The circumstellar emission region is clearly extended and closely resembles a symmetrical Gaussian shape with a width of 2′.1 ± 0′.3. From equation (28) we get $\eta_f = 0.56$, and using the measured $T_A^* = 4.2 \pm 0.5$ K from Table 3 we calculate an excitation temperature of 10.9 ± 1.3 K, assuming the line is optically thick (Wilson *et al.* 1973).

Maps of the $^{12}C^{16}O$ emission from the Orion Nebula (Liszt *et al.* 1974) are dominated by a central 4′ × 9′ ridge. Assuming a Gaussian profile with widths of 4′ in right ascension and 9′ in declination, we calculate $\eta_f = 0.69$ from equation (28). If the $^{12}C^{16}O$ line is optically thick, our $T_A^* = 60.0 \pm 4.7$ K indicates an excitation temperature of 91 ± 7 K. Liszt *et al.* (1974) independently measured a peak antenna temperature of 30 K for the $^{12}C^{16}O$ line in Orion A, also using the NRAO 11 m telescope. Correcting for atmospheric absorption and antenna losses results in a $T_A^* = 57$ K, which agrees with our measurement. Our value for the excitation temperature is higher than the 75 K calculated by Liszt *et al.* (1974), because we have corrected for the microwave background radiation and also for the power lost in the wings of the error pattern. Similar observations of $^{12}C^{16}O$ in Orion A with The University of Texas 5 m antenna resulted in a $T_A^* = 72$ K (Davis and Vanden Bout 1973), a value 20 percent greater than the $T_A^* = 60$ K we measured on the NRAO telescope. The Texas antenna has a more precise reflecting surface than the NRAO dish (Ulich *et al.* 1973), and consequently less power is received in the error pattern and more power is concentrated in the main lobe. Therefore, for sources larger than either main beam, n_f (and T_A^*) will be larger for the Texas antenna, even though it is less than half the diameter of the NRAO telescope. We estimate that at 2.6 mm wavelength the Texas antenna parameters are $\theta_D = 2'.2$, $\theta_E = 25'$, $A_D = 0.9997$, and $A_E = 3 \times 10^{-4}$. For Orion A $n_f = 0.82$ and the corresponding excitation temperature is also 91 K. Thus independent measurements on the two antennas are in complete agreement once the proper corrections are made for the effects of the error patterns on the forward beam coupling efficiencies.

As a further check on the accuracy of the chopper-wheel calibration method we observed a very extended uniformly bright source. Maps of the $^{12}C^{16}O$ emission near R CrA ($\alpha_{1950} = 18^h59^m32^s.8$, $\delta_{1950} = -37°14'8''$) with the Texas antenna indicate relatively uniform emission over a region larger than 1° in diameter and a $T_A^* = 15.4$ K at the calibration position (Loren 1975). For uniform sources much larger than the error pattern width, $\eta_f = 1.00$ for both telescopes, and one expects to measure identical values of T_A^*. With the NRAO telescope we measured 15.3 ± 0.7 K (here the error is due to random receiver noise only), which is in fact essentially identical to the Texas result. Thus the chopper-wheel calibration method accurately corrects for all antenna losses.

In this paper we have analyzed the chopper-wheel calibration scheme and reported observations with a unique radiometer which is capable of accurate absolute intensity measurements. We have calibrated six spectral lines in the 3.5 mm to 2.6 mm wavelength range using the NRAO 11 m telescope. The results are shown to be consistent with independent absolute continuum observations and with other spectral line data taken with both the NRAO and Texas radio telescopes. We have also shown that apparent discrepancies in the corrected antenna temperatures measured with the two antennas are reconciled when corrections are made for the effects of the antenna error patterns.

REFERENCES

Ade, P. A. R., Rather, J. D. G., and Clegg, P. E. 1974, *Ap. J.*, **187**, 389.
Baars, J. W. M. 1973, *IEEE Trans.*, ***AP*-21**, 461.
Buhl, D., and Snyder, L. E. 1970, *Nature*, **228**, 267.
———. 1973, *Ap. J.*, **180**, 791.
Davis, J. H., and Vanden Bout, P. 1973, *Ap. Letters*, **15**, 43.
Harten, R. H. 1973, *A.J.*, **78**, 565.
Klemperer, W. 1970, *Nature*, **227**, 1230.
Liszt, H. S., Wilson, R. W., Penzias, A. A., Jefferts, K. B., Wannier, P. G., and Solomon, P. M. 1974, *Ap. J.*, **190**, 557.
Litvak, M. M. 1971, *Ap. J.*, **170**, 71.

Loren, R. 1975, private communication.
Penzias, A. A. 1972, *Cosmology, Fusion, and Other Matters* (Boulder: Colorado Associated University Press), p. 29.
Penzias, A. A., and Burrus, C. A. 1973, *Ann. Rev. Astr. and Ap.*, **11**, 51.
Ruze, J. 1966, *Proc. IEEE*, **54**, 633.
Snyder, L. E., and Buhl, D. 1971, *Ap. J. (Letters)*, **163**, L47.
———. 1974, *ibid.*, **189**, L31.
———. 1975, *Ap. J.*, **197**, 329.
Snyder, L. E., Hollis, J. M., Ulich, B. L., Lovas, F. J., and Buhl, D. 1975*a*, *Bull. AAS*, **7**, 497.
Snyder, L. E., Hollis, J. M., Ulich, B. L., Lovas, F. J., Johnson, D. R., and Buhl, D. 1975*b*, *Ap. J. (Letters)*, **198**, L81.
Tolbert, C. W., Krause, L. C., and Straiton, A. W. 1964, *J. Geophys. Res.*, **69**, 1349.
Ulich, B. L. 1974, *Icarus*, **21**, 254.
Ulich, B. L., Cogdell, J. R., and Davis, J. H. 1973, *Icarus*, **19**, 59.
———. 1974, *Moon*, **10**, 163.
Waters, J. W. 1975, private communication.
Wilson, R. W., Jefferts, K. B., and Penzias, A. A. 1970, *Ap. J. (Letters)*, **161**, L43.
Wilson, W. J., Schwartz, P. R., and Epstein, E. E. 1973, *Ap. J.*, **183**, 871.
Zuckerman, B., and Palmer, P. 1974, *Ann. Rev. Astr. and Ap.*, **12**, 279.

B. L. ULICH: National Radio Astronomy Observatory, Suite 100, 2010 N. Forbes Blvd., Tucson, AZ 85705

R. W. HAAS: Max-Planck-Institut für Radioastronomie, D-5300 Bonn 1, Auf dem Hügel 69, Federal Republic of Germany